Solar Physics (2005) 228: 137–148

FILAMENT RECOGNITION IN SOLAR IMAGES WITH THE NEURAL NETWORK TECHNIQUE

V. V. ZHARKOVA
Department of Cybernetics, University of Bradford, BD7 1DP, U.K.
(e-mail: V.V.Zharkova@brad.ac.uk)

and

V. SCHETININ
Department of Computer Science, University of Exeter, EX4 4QF, U.K.
(e-mail: V.Schetinin@ex.ac.uk)

(Received 31 January 2005; accepted 15 March 2005)

Abstract. We describe a new technique developed for an automated recognition of solar filaments visible in Hα hydrogen line full-disk spectroheliograms. These filaments are difficult to recognize because of variability in the background caused by atmospheric conditions. The presented technique is based on an artificial neural network (ANN) consisting of two hidden neurons and one output neuron which learn to exclude the contribution of a changeable background to a filament. The ANN is trained on a single image fragment labeled manually to recognize the filament elements depicted on a local background. The background contribution is approximated with linear and parabolic functions. This technique applied to the filament recognition in 54 cropped images reveals better detection results for a parabolic approximation than for a linear one approaching an accuracy of about 82% of the total filament pixels.

1. Introduction

Solar images observed from the ground and space-based observatories at various wavelengths are digitized and stored in different catalogues, which are to be unified under the grid technology program. Robust techniques including limb fitting, removal of geometrical distortion, center position, size standardization and intensity normalization have been developed to standardize the full-disk images taken in Hα and Ca K1-K3 lines taken at the Meudon Observatory (France) (Zharkova *et al.*, 2003a). There is a growing interest in wide-spread ground-based daily observations of full solar disk images in the Hα line, which can provide important information on long-term solar activity variations during months or years. The European Grid of Solar Observations project (Bentley *et al.*, 2002) was designed to provide automated detection of various features associated with solar activity such as sunspots, active regions and filaments or solar prominences.

Filaments are dark elongated features seen in absorption, which are the projections on the solar disk of prominences seen on the solar limb as very bright and large-scale features (Zharkova *et al.*, 2003a). Their location and shape does not change very much for a long time and, hence, their lifetime is likely to be

much longer than one solar rotation. However, there are visible changes seen in the filament elongation position with respect to an active region and magnetic field configuration. For this reason the automated detection of solar filaments is a very important task to tackle for understanding the physics of prominence formation, support and disruption. Recently, two techniques were applied for feature detection: rough detection with a mosaic threshold (MT) technique (Zharkova *et al.*, 2003b; Qahwaji and Green, 2001) and the image segmentation and region growing (RG) techniques (Bader *et al.*, 1996; Fuller, Aboudarham, and Bentley, 2005; Gao, Zhou, and Wang, 2001; Turmon, Mukhtar, and Pap, 1997, 1998). However, these techniques are strongly dependent on the background standardization procedures (Zharkova *et al.*, 2003a) that exclude limb darkening and Gaussian noise. Most techniques but the RG one (Fuller, Aboudarham, and Bentley, 2005) are also not suitable for automated feature classification, which is an important task for future solar data processing. However, region growing performs well only on standardized images with their intensity and shape corrected with the technique described by Zharkova *et al*. (2003a). Normally, this is a rather lengthy process of about 10 min per image that is the price paid for the high accuracy detection of about 90% (Fuller, Aboudarham, and Bentley, 2005).

In order to speed up the filament detection process in solar images with their intensities not being standardized, Artificial Neural Network (ANN) techniques (Bishop, 1995; Nabney, 2001) can be applied if there is a representative set of the image data available with the filaments marked. Such a training data set has to include an exhaustive set of filaments depicted on different backgrounds whose brightness and other visual parameters vary over a full range. The background variations are associated either with different absorption profiles for the radiation emitted from various parts of the solar disk in a two-dimensional (flat) solar image (from the center to the limb called the limb darkening), or by varying seeing conditions during the observations caused by weather, atmosphere transparency etc. However, the image fragments are still labeled manually which limits the number of training examples and reduces the statistical values of the training set.

The proposed ANN consists of two hidden neurons and one output neuron. These neurons learn to exclude the contributions of a variable background to a filament. In a small area, the background contribution can be approximated by a linear function (Zharkova and Schetinin, 2003) and the ANN has revealed acceptable accuracy recognizing filaments around the central areas of a solar disk not much affected by the limb darkening. However, for a larger area and areas closer to the solar limb the background contribution is better approximated by a parabolic function according to the limb darkening formula (Allen, 1973). In such cases, the ANN provides more accurate recognition of the filaments.

The motivation for the presented paper is to develop a new ANN technique for filament recognition on a variable background and compare its performance for linear and parabolic approximations. The general recognition problem with ANN

is formulated in Section 2. The new ANN technique developed for the recognition of solar filaments is described in Section 3, the training method is described in Section 4. Discussion of the detection results obtained with the new ANN method is described in Section 5 and conclusions are drawn in Section 6.

2. The Recognition Problem

The image of the solar disk can be split into separate rectangular fragments each containing one or more filaments. Since these image fragments come from different parts of the solar disk, their brightness varies from fragment to fragment and even within a fragment dependent on the observation conditions and instrumental errors.

Let us define an image fragment data as the $(n \times m)$ matrix $\mathbf{X} = \{x_{ij}\}$, $i = 1, \ldots, n, j = 1, \ldots, m$, consisting of pixels whose brightness ranges between 1 and 255. This fragment depicts a filament which is a dark elongated feature observable on a background with relatively higher brightness. Within the fragment, the pixel x_{ij} can belong either to *a filament region*, class Ω_0, or to a *non-filament region*, class Ω_1. Hence, the recognition problem is to distinguish pixels of the given fragment between the classes Ω_0 and Ω_1.

Now let us define *a background function* $u_{ij} = \varphi(\mathbf{X}; i, j)$ which reflects the brightness u_{ij} of pixel x_{ij} taken from a given image $\mathbf{X}$ in a position $\langle i,\ j\rangle$. As the brightness of a pixel may depend on its position $\langle i,\ j\rangle$, this function has to satisfy one of the following two properties:

$$\varphi(\mathbf{X};\ i,\ j) = \varphi \quad \forall i = 1,\ \ldots,\ n,\ j = 1,\ \ldots,\ m, \tag{1}$$

$$|\Delta\varphi_{ij}| > 0, \tag{2}$$

where $\varphi_0 \geq 0$ is a constant and $\Delta\varphi_{ij}$ is a finite difference for the function φ.

The first property is referred to a case when the variability of background elements is non-distinguishable and the contribution of background to any pixel value x_{ij} in the image $\mathbf{X}$ is a constant. The second property is referred to an alternative case when within some neighborhood of pixel x_{ij} the background elements make different contributions to the brightness of this pixel.

A structure for the background function φ can be predefined and its parameters fitted to a given image $\mathbf{X}$. The output of this function, u_{ij}, calculated for all the pixels of $\mathbf{X}$ could be used to exclude the contribution of a variable background to the filament if this contribution can be assumed as additive. Additionally, it is assumed that a pixel x_{ij} can be affected by neighboring background elements within a rectangular window $\mathbf{P}$ consisting of $(k \times k)$ elements.

So, using the above assumptions, the influence of a variable background on the brightness of a central pixel of the window $\mathbf{P}$ in each position $\langle i,\ j\rangle$, $i = 1, \ldots, n$, $j = 1, \ldots, m$, can be excluded as follows. The output u_{ij} of function φ calculated for the element $\langle i,\ j\rangle$ is subtracted from the pixel brightness x_{ij}.

3. The Neural-Network Technique for Filament Recognition

In order to estimate the background function in a given image **X**, the rectangular window **P** is used, which is a $(k \times k)$ matrix containing the central pixel x_{ij} and $r-1$ nearest pixels, where $r = k^2$. Then by sliding the window **P** through the image **X**, every central pixel x_{ij} in the **P** can be assigned to one of the two classes, Ω_0 or Ω_1. The use of such a sliding technique aims to transform the original image **X** into a $(r \times q)$ matrix **Z** with the columns $(\mathbf{z}^{(1)}, \ldots, \mathbf{z}^{(q)})$, where $q = (n-k+1)(m-k+1)$ is the number of columns. Each column consists of r elements of matrix **P** so that the central element of **P** is located in the $(r+1)/2$ position of the column. An example of sliding is presented in Figure 1 for the case when **X** is a (4×5)-matrix, $k = 3$, and **P** is a (3×3)-matrix. For this case $r = 9$, $q = 6$, and **Z** is a (9×6)-matrix of which the columns $(\mathbf{z}^{(1)}, \ldots, \mathbf{z}^{(q)})$ are the elements of matrix **P** taken subsequently at positions $\langle 2,\ 2\rangle, \langle 2,\ 3\rangle, \ldots, \langle 3,\ 3\rangle, \langle 3,\ 4\rangle$ of the original matrix X; each of these positions corresponds to the tth column of matrix **Z**, $t = 1, \ldots, 6$.

For the matrix **Z**, the output of a background function can be written as a function $u_t = \varphi(t)$, $t = 1, \ldots, q$, which is the contribution of the r background elements containing in column $\mathbf{z}^{(t)}$ at a position of the sliding window on the image. Therefore, for matrix **Z**, the properties (1) and (2) can be rewritten as follows:

$$\varphi(t) = \varphi_0 \quad \forall t = 1, \ldots, q, \tag{3}$$

$$|\Delta\varphi_t| > 0. \tag{4}$$

In general, there are several functions, which can match the properties (3) and (4). One is a linear function $u_t = \alpha_0 + \alpha_1 t$, where α_0 and α_1 are the coefficients.

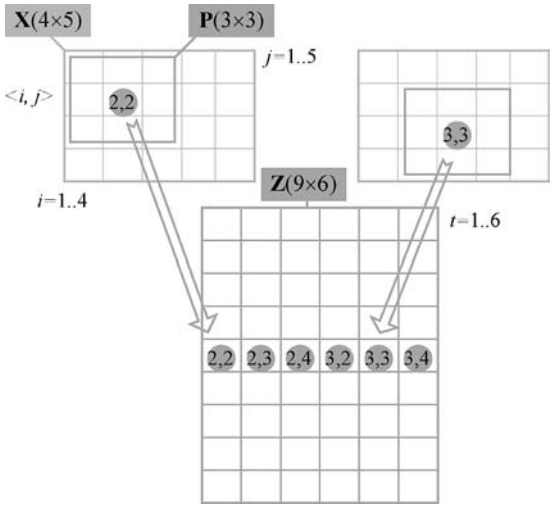

Figure 1. Transformation of the original image **X** (4×5) into the matrix **Z** (9×6) by using a window **P** (3×3). The circles are central pixels of the window **P** at the positions $\langle 2, 2\rangle, \ldots, \langle 3, 4\rangle$.

Indeed, the property (3) is satisfied if the contribution of the background elements is described as $u_t = \alpha_0$, and it is not dependent on the position t. Property (4) is satisfied when the contribution is linearly dependent on the index t. In this case the finite difference $\Delta\varphi_t = \alpha_1$.

Another function which can satisfy (3) and (4) is a parabolic one. This function is more suitable for large image fragments, when the variation in brightness of pixels cannot be assumed linear due to projecting a solar sphere on a two-dimensional image. In this case the contribution of background elements can be described as

$$u_t = U(\alpha; t) = \alpha_0 + \alpha_1 t + \alpha_2 t^2, \tag{5}$$

where α is the vector of coefficients.

In both cases the coefficients of the linear and parabolic approximations are fitted to the image data so that the squared error e becomes minimal:

$$e = \sum_{t=1}^{q} \left[U(\alpha; t) - \beta_0 - \sum_{i=1}^{r} \beta_i z_i^{(t)} \right]^2, \tag{6}$$

where $\beta_i > 0$ are the coefficients given on the pixels taken from the tth column of matrix $\mathbf{Z}$ and β_0 is the bias.

Note that the weighted sum over r elements of the column $\mathbf{z}^{(t)}$ operates as a filter suppressing the influence of a background noise on each central pixel. At the same time, this sum estimates the contribution of $r - 1$ neighboring elements to the central element. The coefficients $\alpha_0, \ldots, \alpha_2$ in (6) can be fitted by using a least square error method (Bishop, 1995; Nabney, 2001).

The above idea can be implemented within a feed-forward ANN consisting of two hidden neurons and one output neuron as depicted in Figure 2.

The first hidden neuron, f_1, fed by the r elements of the tth column $\mathbf{z}^{(t)}$ estimates their contribution s_t to the central element. The second hidden neuron, f_2, estimates the contribution of the local background u_t to this element. The output neuron, f_3, makes a final decision $y_t = \{0, 1\}$ on the central element at the column $\mathbf{z}^{(t)}$.

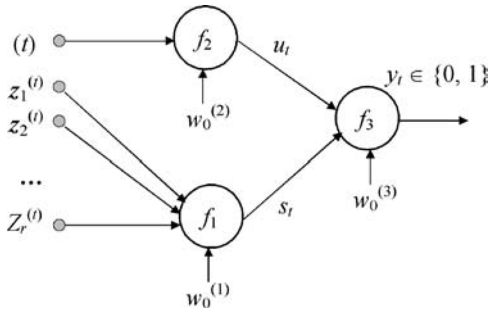

Figure 2. The feed-forward ANN consisting of two hidden neurons and one output neuron used for filament recognition.

For each column $\mathbf{z}^{(t)}$, the output s_t of the first hidden neuron is calculated as follows:

$$s_t = f_1\left(w_0^{(1)}, \mathbf{w}^{(1)}; \mathbf{z}(t)\right), \quad t = 1, \ldots, q, \tag{7}$$

where $w_0^{(1)}$, $\mathbf{w}^{(1)}$, and f_1 are the bias term, weight vector and an activation function of the neuron, respectively.

The activity of the second hidden neuron reflects the contribution of the background elements to the central pixel of the vector $\mathbf{z}^{(t)}$ and can be written as follows:

$$u_t = f_2\left(w_0^{(2)}, \mathbf{w}^{(2)}; t\right), \quad t = 1, \ldots, q, \tag{8}$$

where f_2 is the activation function, a linear or parabolic as described above.

The bias term $w_0^{(2)}$ and the weight vector $\mathbf{w}^{(2)}$ of this neuron are fitted so that the approximation error (6) becomes minimal.

Taking into account the values of s_t and u_t, the output neuron makes a final decision $y_t \in \{0, 1\}$ for a central pixel of vector $\mathbf{z}^{(t)}$ as follows:

$$y_t = f_3\left(w_0^{(3)}, \mathbf{w}^{(3)}; s_t, u_t\right), \quad t = 1, \ldots, q. \tag{9}$$

Depending on outputs of the hidden neurons, the output neuron assigns a central pixel of the vector $\mathbf{z}^{(t)}$ either to the class Ω_0 or Ω_1. Thus, processing all q elements of matrix $\mathbf{Z}$, the ANN distinguishes between the filament and background elements.

4. The Training Algorithm

The ANN depicted in Figure 2 can be trained with the standard back-propagation technique aimed to minimize an error function for a given number of the training epochs. During the training this technique repeatedly updates weights of the hidden neurons and then calculates their outputs for all q columns of the matrix $\mathbf{Z}$. Clearly, this technique, which searches for a global optimum, is computationally expensive. However, there are some local solutions which can be found while the hidden and output neurons are trained separately. Providing an acceptable accuracy, such solutions may be found much more easily than the global one. The training algorithm based on such a local solution is described below.

First we need to fit the weight vector of the second hidden, or "background" neuron, which evaluates the contribution of the background elements. The contribution of these elements to a brightness of filament element is dependent on many factors, including the limb darkening (Allen, 1973), weather conditions and instrumental errors.

Let error e_t be calculated as follows:

$$e_t = s_t - u_t, \tag{10}$$

and define the function f_1 as a linear function:

$$s_t = w_0^{(1)} + \sum_{i=1}^{r} w_i^{(1)} z_i^{(t)}, \quad t = 1, \ldots, q, \tag{11}$$

with the coefficients $w_0^{(1)}, \ldots, w_r^{(1)}$.

The local solution, which we are interested in, was found by setting the weights $w_i^{(1)}$, $w_0^{(1)}$ to be equal to 1 and 0, respectively. With such values the ANN performed well in our experiments.

The background function u_t can be defined as a linear or parabolic:

$$u_t = w_0^{(2)} + w_1^{(2)} t, \tag{12a}$$

$$u_t = w_0^{(2)} + w_1^{(2)} t + w_2^{(2)} t^2. \tag{12b}$$

The weight coefficients $w_0^{(2)}$, $w_1^{(2)}$, and $w_2^{(2)}$ of this neuron are fitted to the data $\mathbf{Z}$ so that the sum squared error E between the outputs u_t and s_t is minimal:

$$E = \sum_t (u_t - s_t)^2 = \sum_t \left(w_0^{(2)} + w_1^{(2)} t + w_2^{(2)} t^2 - s_t\right)^2 \to \min, \quad t = 1, \ldots, q. \tag{13}$$

The desirable weight coefficients $w_0^{(2)}, \ldots, w_2^{(2)}$ can be estimated by the least square error method (Bishop, 1995; Nabney, 2001). Thus, the "background" neuron is trained to evaluate the contribution of background elements to each column $\mathbf{z}^{(t)}$. Note that the weights $w_0^{(2)}, \ldots, w_2^{(2)}$ are evaluated for every image and consequently the "background" neuron is retrained each time.

Having defined the weights for both hidden neurons, now it is possible to train the output neuron, which assigns the central pixel of the column $\mathbf{z}^{(t)}$ to one of the two classes. The output y_t of this neuron is described as follows:

$$\begin{aligned} &y_t = 0 \quad \text{if } w_0^{(3)} + w_1^{(3)} s_t + w_2^{(3)} u_t < 0, \\ &y_t = 1 \quad \text{otherwise.} \end{aligned} \tag{14}$$

The weights of the output neuron can be fitted so that the recognition error E_r is minimal:

$$E_r = \sum_i |y_i - t_i| \to \min, \quad i = 1, \ldots, h, \tag{15}$$

where $|\cdot|$ takes an absolute value, $t_i \in \{0, 1\}$ is the class given on the i-th training example and h is a number of the training examples.

The desirable values of $w_0^{(3)}$, $w_1^{(3)}$ and $w_2^{(3)}$, which provide a minimum of the error (15), can be achieved by using the standard learning methods under the assumption of a Gaussian noise in the data (Nabney, 2001). In the case, if the noise in the image data is not Gaussian, one can apply another learning algorithm described by Schetinin (2003).

The results of the training can be improved, if the weights $w_1^{(3)}$ and $w_2^{(3)}$ are set equal to 1.0 and -1.0, respectively, and only one parameter, the bias $w_0^{(3)}$, is fitted. Then the input s_t' of the third neuron can be normalized to be with zero mean and unit variance as follows:

$$s_t' = \frac{e_t - M_e}{\left[1/q \sum_{i=1}^{q} (e_i - M_e)^2\right]^{1/2}}, \quad t = 1, \ldots, q, \tag{16}$$

where $M_e = 1/q \sum_{t=1}^{q} e_t$ is the mean value of e_t.

5. Results and Discussion

The neural network consisting of two hidden neurons and one output neuron was developed to recognize filaments visible in Hα line full-disk spectroheliograms. These images were obtained at the Meudon Observatory (France) during March–April 2002. 55 image fragments with filaments were taken from several regions from the full-disk images. These images have varying brightness because of the limb darkening, instrumental errors and different observation conditions.

For training one cropped image fragment was visually labeled by an expert. Figures 3 and 4 plot the examples of the linear and parabolic approximations of a background contribution. The top left plots in these figures depict the original images presenting two different filaments on the unknown background. The first

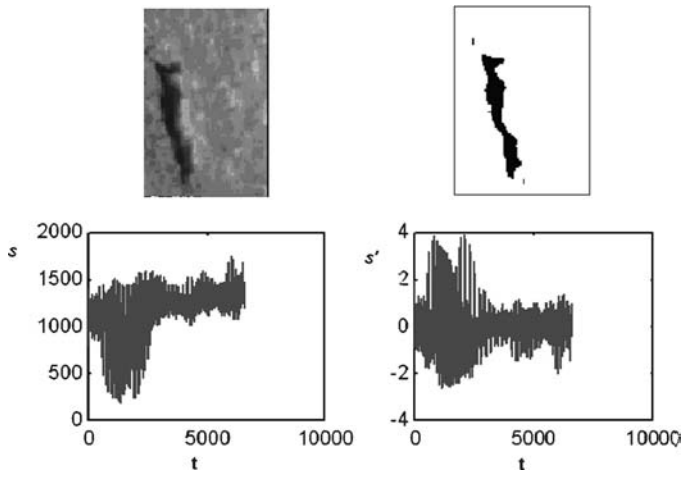

Figure 3. Example of a small filament (*the top left plot*) affected by the background seen as a linear trend in the values of s_t (*the bottom left plot*). The filament recognized with a linear approximation (*the top right plot*) and the normalized output s_t' in which the background contribution was excluded (*the bottom right plot*).

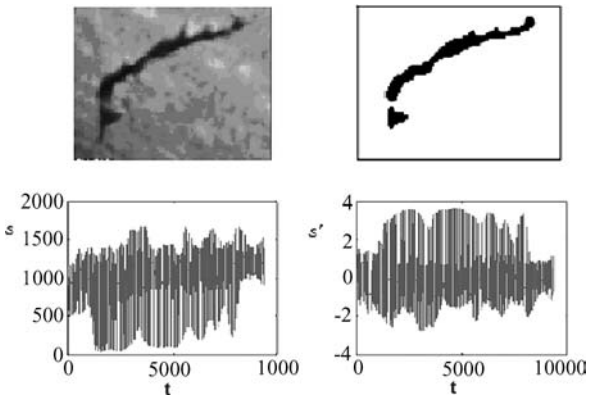

Figure 4. Example of a large filament (*the top left plot*) affected by the background seen as a flat parabolic trend in the values of s_t (*the bottom left plot*). The filament recognized with a linear approximation (*the top right plot*) and the normalized output s'_t in which the background contribution was excluded (*the bottom right plot*).

filament (Figure 3) is relatively small and consists of 6.9 K pixels, and the second one (Figure 4) is larger and contains 12.2 K pixels.

The bottom left plots in Figures 3 and 4 depict the output s_t when the background function is not taken into account yet. The scale of the s_t is large, up to 1700 in both figures. Among the values of s_t depicted in Figure 3 there is seen a linear trend over $t = 1, \ldots, q$, that allows the linear background function (12a) to apply. The normalized output s'_t shows that the linear approximation works well and the background contribution seen as a linear trend is excluded.

For larger filaments as depicted at the top left plot in Figure 4, the background varies more significantly than for smaller filaments as it is seen at the bottom left plot. This filament is located closer to the solar limb and its elements are more strongly affected by the limb darkening. In this case the background contribution is better approximated by a parabolic function as the normalized function s'_t shows at the bottom right plot.

Hence, by comparing the resultant filaments in Figures 3 and 4, one can conclude that the background neurons have been successfully trained to exclude the background contributions with both the linear and parabolic approximations. The recognized filament elements marked in black in the top right plots of Figures 3 and 4 match the original filaments rather well.

Trained on these filament pixels for the linear and parabolic background approximations, the proposed technique was used for filament recognition in another 54 fragments. The recognition results for multiple filaments of different sizes on a strongly variable background are depicted at the left plot in Figure 5. The middle plot shows that the ANN with a linear approximation cannot recognize correctly the filaments and detects more than those were really presented. This happens because the background brightness varies widely and some dark background elements at

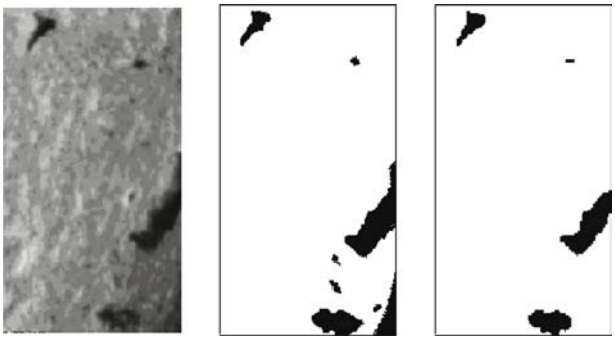

Figure 5. The original fragment with multiple filaments (*the left plot*), the resultant filaments obtained with the linear (*the middle plot*) and parabolic (*the right plot*) approximations.

the bottom right edge at the left plot are recognized as the filaments seen at the middle plot in Figure 5. The ANN trained with a parabolic approximation recognizes the filament elements at the right plot in Figure 5 much better. One can see that the locations and shapes of all the filaments are recognized rather well. The misclassifications were mainly caused by shrinkage of the recognized filaments.

Comparing the above results, one can see that when large fragments contain multiple filaments the parabolic approximation provides better performance than that with a linear approximation. The remaining 54 fragments were labeled by using the automated RG technique (Fuller, Aboudarham, and Bentley, 2005) that has a high detection accuracy of 90%. From a comparison of our detection results with those by the RG method, the total classification accuracy on the test data is about 75% for linear and 82.5% for parabolic background functions.

A challenging task will be to process larger fragments as full-disk images and is not implemented yet; this is a subject of a future paper. Another question is the computational time required by the proposed ANN method. This method was implemented with Matlab and Matlab Image Processing Tool with the processing time for a fragment not exceeding 0.5 s. This time is significantly shorter than 20 min for the RG method (Fuller, Aboudarham, and Bentley, 2005) but 5-times longer than 0.01 s for the MT method (Zharkova *et al.*, 2003b). The processing time can be significantly improved by using C/C++ code techniques that are also planned for in the future work. However, keeping in mind the very reasonable accuracy of detection with ANN that is comparable with the RG method, the ANN method provides a very efficient approach to filament detection.

6. Conclusions

The automated recognition of filaments in solar images is still a difficult problem because of the background variation caused by limb darkening, instrumental

errors and inhomogeneities in the terrestrial atmosphere during observations. The proposed technique exploits an ANN consisting of two hidden neurons and one output neuron with one hidden neuron learning to exclude a variable background contribution. The ANN was trained to recognize solar filaments on a single image fragment whose pixels were labeled manually. The background contribution was approximated with the linear and parabolic functions.

Despite the difference in the backgrounds, the ANN has properly recognized both single and multiple filaments presented in the image fragments. The use of the parabolic approximation allows large filaments to be recognized more accurately than with the linear approximation. In general, the resultant ANN has successfully recognized the filaments in the 54 other fragments depicted on a variable background. The classification accuracy for the parabolic approximation is about 82.5% which is higher than for the linear one (75%) and 9% lower than those obtained with the accurate region growing method (Fuller, Aboudarham, and Bentley, 2005). Thus, we conclude that the proposed ANN technique can be effectively used for automated recognition of filaments in solar images.

Acknowledgements

The authors would like to thank referee Pietro N. Bernasconi for his constructive comments. We are also thankful to Jonathan E. Fieldsend (Exeter University, U.K.) for useful discussion. This research was supported by the project European Grid of Solar Observations (EGSO), funded by the European Commission, Grant IST-2001-32409 (VZ) and by EPSRC, Grant GR/R24357/01 (VS).

References

Allen, C. W.: 1973, *Astrophysical Quantities*, Athlone Press, London.

Bader, D. A., Jaja, J., Harwood, D., and Davis, L. S.: 1996, *Proc. IEEE IPPS'96*, p. 414.

Bentley, R. D. and EGSO Consortium: 2002, *Proc. of the 10th European Solar Physics Meeting*, 9–14 September, 2002, Prague, Czech Republic, A. Wilson (ed.), ESA SP-506, Vol. 2, ISBN 92-9092-816-6, p. 923.

Bishop, C. M.: 1995, *Neural Networks for Pattern Recognition*, Oxford University Press, p. 504.

Fuller, N., Aboudarham, J., and Bentley, R. D., 2005, *Solar Phys*., in press.

Gao, J., Zhou, M., and Wang, H.: 2001, *Proc. Information Science and Systems,* Johns Hopkins University, p. 401.

Nabney, I. T., NETLAB: 2001, *Algorithms for Pattern Recognition*, Springer-Verlag, p. 420.

Qahwaji, R. and Green, R.: 2001, *Int. J. Comput. Their Appl.* **8**, N4, 202.

Schetinin, V.: 2003, *Neural Proce. Lett.* **17**, 21.

Turmon, M., Mukhtar, S., and Pap, J.: 1997, *Proc. Knowledge Discovery and Data Mining*, p. 237.

Turmon, M., Pap, J., and Mukhtar, S.: 1998, *Proc. Structure and Dynamics of the Interior of the Sun and Sun-like Stars*, Boston, p. 117.

Zharkova, V. V. and Schetinin, V.: 2003, *Proc. 8th Int. Conf. Knowledge-Based Intelligent Information and Engineering Systems (KES2003)*, Part I, ISBN 3-540-40804-5, p. 148.

Zharkova, V. V., Ipson, S. S., Zharkov, S. I., Benkhalil, A., Aboudarham, J., and Bentley, R. D.: 2003a, *Solar Phys*. **214**, 89.

Zharkova, V. V., Ipson, S. S., Qahwaji, R., Zharkov, S., and Benkhalil, A.: 2003b, *Proc. SMMSP-2003*, Barcelona, Spain, 115.